JOURNAL OF COMPUTATIONAL PHYSICS 74, 283–317 (1988)

Validation Study of Vortex Methods*

J. A. SETHIAN

Department of Mathematics, University of California Berkeley, Berkeley, California 94720

AND

AHMED F. GHONIEM

Department of Mechanical Engineering, Massachusetts Institute of Technology, Cambridge, Massachusetts 01239

Received June 2, 1986; revised March 25, 1987

Convergence of the vortex method applied to viscous, incompressible flow is demonstrated. We compute the solution of flow over a backwards-facing step for Reynolds number 50, 125, 250, 375, 500, and 5000, and study the effect of the choice of numerical parameters on the accuracy of the computed solution. Within the laminar regime, we demonstrate convergence of the computed means to a time-independent solution as the numerical parameters are refined, decay of variance around the computed mean inversely proportional to the number of vortex elements, and accurate comparison of size and length of recirculation zones with experimental measurements as a function of Reynolds number. At higher Reynolds number, we show detailed and robust calculations of eddy shedding and pairing, and qualitative numerical convergence in such flow variables as eddy size and average velocity profiles.
© 1988 Academic Press, Inc.

I. INTRODUCTION

In this paper, we present a careful and detailed study of the accuracy of the vortex method applied to viscous, incompressible flow. The goal is to analyze the effect of the choice of time step, number of particles, boundary layer resolution, core size, and domain truncation length on the computed solution. The test problem we model is flow over a backwards-facing step over a wide range of Reynolds numbers, chosen because of the wealth of experimental data available. Since the vortex method is a statistical method, we measure decay of variance and

* This work was supported in part by the Applied Mathematics Subprogram of the Office of Energy Research, U. S. Department of Energy under Contract DE-AC03-76SF00098, the National Science Foundation under the National Science Foundation Mathematical Sciences Post-Doctoral Fellowship Program, the National Science Foundation Grant CPE-8404811, and the Air Force Office of Scientific Research under Grant AFOSR84-0356.

0021-9991/88 $3.00
Copyright © 1988 by Academic Press, Inc.
All rights of reproduction in any form reserved.

convergence of the means as the numerical parameters are refined. In the laminar regime, where physical experiments indicate a steady, stable, recirculating profile, we show

(1) decay of variance around computed means inversely proportional to the number of vortex elements

(2) pointwise convergence of the computed means to a time-independent profile

(3) prediction of the experimentally measured relationship between Reynolds number and the size and length of the recirculation zone

(4) accuracy dependent primarily on the number of vortex elements, and the secondary importance of time step, boundary layer resolution, etc.

In the transitional regime, physical experiments indicate an unsteady mechanism of eddy shedding downstream of the recirculation bubble, and coherent traveling eddy structures. Here, we show

(1) prediction of the qualitative large-scale mechanism of the flow dynamics, which remains unchanged as the numerical parameters are refined

(2) numerical convergence of integrated, global quantities (eddy size, shape, average velocity profiles)

(3) primary accuracy dependence on the number of vortex elements, and a critical empirical relationship between the number of elements and the time step.

To summarize, throughout the laminar regime we demonstrate convergence of the method as the numerical parameters are refined, and in the transitional-turbulent regime, we accurately predict the large-scale global dynamics of the flow, whose properties remain unchanged with refinement of numerical parameters.

The vortex method relies on a discretization of the continuous time-dependent vorticity field into a large number of interacting vortex "blobs," whose position and strengths determine the underlying velocity field. This method has gained considerable popularity in recent years and has been used in a variety of settings (see [4, 9, 10, 17, 18, 27, 30, 33, 35, 41, 42, 43, 44]). Previous applications have focused on predicting gross qualitative structures of highly turbulent flow. To the best of our knowledge, detailed convergence studies of the accuracy of the computed solution as a function of numerical parameters have never been performed. In applying the method to high Reynolds number flow, trying to determine how to assess convergence is made difficult by the unsteady, turbulent nature of the flow. Thus, before we move to larger Reynolds numbers, we start our study at low Reynolds numbers, where the method may not be very efficient, but where the flow is stable and steady.

We study the two-dimensional Navier–Stokes equations, which is a significant restriction that ignores such three-dimensional effects as vortex stretching. Thus we must use caution in comparing our two-dimensional calculations with experiment.

Our point of view is that at low Reynolds numbers, results are indeed two-dimensional, and that analysis of the 2D Navier–Stokes equations from low to moderate Reynolds number can provide insight into the transition from steady to unsteady flow. Thus, with respect to our calculations, the word "turbulent" shall mean the instability of small-scale flow and the resulting coagulation of vorticity into large fluid structures that comes with increasing Reynolds number.

In practice, there are several ways to speed up the vortex method, most notably through the use of fast Poisson solvers, near-field/far-field techniques, boundary layer interpolating splines, etc. We do not use these techniques, because we want to study the basic random vortex method with as few numerical parameters as possible; labor-saving techniques would have introduced even more numerical parameters. This numerical convergence study required several thousand hours of computer time and generated massive amounts of data, enough to fill seventeen 6250 bpi tapes. Not surprisingly, we were forced to confront the related issue of developing an organized and effective way of looking at that much data, and this will be the subject of a later paper [40].

II. Equations of Motion

The momentum equation for two-dimensional, viscous, incompressible flow [29] is

$$\frac{D\mathbf{u}}{Dt} = \frac{1}{R}\nabla^2\mathbf{u} - \nabla P, \tag{1}$$

where $\mathbf{u} = (u, v)$ is the velocity of the fluid, D/Dt is the total derivative, $P = P(x, y)$ is the pressure, ∇ is the gradient, and ∇^2 is the two-dimensional Laplacian. Taking the curl of Eq. (1) results in the vorticity transport equation [29]

$$\partial_t \xi + (\mathbf{u}\cdot\nabla)\xi = (1/R)\nabla^2\xi, \tag{2}$$

where the vorticity $\xi = \nabla x \mathbf{u}$, and we have used the fact that if the density is constant, $\nabla x(\nabla P/\rho) = 0$. The flow is incompressible ($\nabla \cdot u = 0$), and on solid walls, $\mathbf{u} = 0$. The computational domain is divided into an interior region and a thin zone near solid walls. The two solutions are matched to produce the full flow. In the interior, the full vorticity transport equation (2) is split into an advection equation $\partial_t \xi = -(\mathbf{u}\cdot\nabla)\xi$, together with the boundary condition $\mathbf{u}\cdot\mathbf{n} = 0$, where $\mathbf{n}$ is the unit vector normal to solid walls, and a diffusion equation $\partial_t \xi = (1/R)\nabla^2\xi$. In the thin zone near the boundary, the Prandtl approximation to the vorticity transport equation is used [29], which is simply a numerical device to allow a transition from one type of discrete vorticity element near the wall to another type away from the wall.

III. The Numerical Scheme

The basic idea behind the numerical scheme, due to Chorin [10, 11], is to update ξ by following the motion of a collection of vortex elements. In the interior, smoothed out point vortices are used (vortex blobs) as the discrete units of vorticity; in the zone near solid walls, discontinuous jumps in the tangential velocity (vortex sheets) are used. Knowledge of the position of the vortex elements at any time provides the velocity field $\mathbf{u}$. We briefly describe the method; for details, see [42].

In the interior, the starting point is vorticity advection equation. If $\mathbf{x}(t)$ is the position of a particle moving in the fluid at time t, then $\xi(\mathbf{x}(t), t) = \xi(\mathbf{x}(0), 0)$. Imagine the initial vorticity approximated by a collection of N particles (vortex "blobs") placed on a grid of grid size h ($N \approx 1/h^2$) covering the domain. Each particle carrys a discrete initial circulation $\xi(\mathbf{x}(i), 0)h^2$, where $\mathbf{x}(i)$ is the initial position of the particle, $1 \leqslant i \leqslant N$. Since $\nabla \cdot \mathbf{u} = 0$, there exists a stream function Ψ such that $\mathbf{u} = (\Psi_y, -\Psi_x)$ and thus $\xi = -\nabla^2 \Psi$. Thus, by using the Green's function for the Laplacian with $\mathbf{x} = (x, y)$, we have

$$\mathbf{u} = \int K(\mathbf{x} - \mathbf{x}')\, \xi(\mathbf{x}', t)\, d\mathbf{x}', \tag{3}$$

where $K(\mathbf{x} - \mathbf{x}') = (-y, x)/(2\pi |\mathbf{x} - \mathbf{x}'|)$. The vortex blob method replaces the singular kernel K by a smoothed kernel K_σ obtained through the convolution $K_\sigma = K * f_\sigma$, where f_σ is a smoothing function. The positions of the vortex blobs are updated in time by numerical integration of the velocity field given in Eq. (3). Convergence of this method was first established in [12, 22]; for work relating to the theoretical aspects of this method, see [2, 5, 6, 12, 20, 22, 23, 24, 38, 39]. In our calculations, we use a second-order time integration scheme (Heun's method) for moving vortex blobs, as suggested in [42].

To update the vorticity with respect to the diffusion term $R^{-1} \nabla^2 \xi$, we allow the vortex elements to undergo a random step, drawn from a Gaussian distribution with mean zero and variance $2\, \Delta t/R$, where Δt is the time step used in the advection scheme. Since a random walk approximates the solution to the diffusion equation, the combined motion of advection plus random step of the vortex blobs approximates the solution to the full vorticity transport equation. For details, see [10]. Similarly, in the zone near the wall, we update the vorticity by advection and random walk of a finite collection of vortex elements. Here, vorticity is approximated by vortex sheets, where a vortex sheet is defined to be a line segment of length h, centered at a point (x_0, y_0) and parallel to the x axis (the wall) such that $u(x_0, y_0^+) - u(x_0, y_0^-) = -\xi$. During one time step, vortex sheets are advanced under the advection field and allowed to undergo a random walk in the direction normal to the wall.

The calculations in the wall zone and the interior are matched as follows: the

velocity from the interior calculation parallel to the wall and a distance δ away is taken as the velocity U_∞ seen at infinity from the numerical boundary layer. As sheets move into the interior, they become blobs and vice versa, and the proper vorticity strength is assigned to the transformed object so that circulation is conserved. This numerical boundary layer of size δ, which is proportional to $1/\sqrt{R}$ for fixed Δt, is merely a mechanism to allow sheets to exist for a few time steps before they turn into blobs; the real edge of the boundary layer will not coincide.

On solid walls, we require that the velocity be zero both normal and tangential to the solid walls. The normal boundary condition is met by finding a function ϕ such that (i) $\nabla^2\phi = 0$ and (ii) $\nabla\phi \cdot \mathbf{n}$ exactly cancels the velocity component normal to solid walls determined by the vortex elements. Approximate entrance and exit requirements on $\nabla\phi \cdot \mathbf{n}$ must also be given. Adding this potential velocity field (ϕ_x, ϕ_y) to the one obtained by the vortex elements provides a velocity field whose normal component vanishes on solid walls. The tangential boundary condition (no-slip condition) along solid walls is met through the creation of vortex sheets as follows. Suppose $\xi_{\max}$ is the maximum amount of vorticity allowed for any one sheet. At the beginning of each time step, calculate the tangential velocity u at points spaced a distance h along the wall. If $u \neq 0$ at any point, create enough vortex sheets to provide a transition from the no-slip condition to the value of u. This ensures that the tangential boundary condition is satisfied at the beginning of each time step. Thus, the interior flow creates vorticity at the boundary due to the no-slip condition, and this vorticity is then diffused from the boundary layer into the interior.

To limit the calculations, we must truncate the channel at some point W_{END} downstream from the step. We delete all the vortex elements past W_{END} and ignore the no-slip condition beyond this point. Thus, infinitely far downstream, we imagine that the flow becomes nearly uniform (independent of x and y). In the calculation presented here, the potential function ϕ is found by a conformal transformation of the domain onto the upper half plane, see [17]: uniform flow conditions are assumed for ϕ at infinity.

IV. Setup of Problem

Let V be a characteristic speed of the incoming flow, let W, the channel height, represent a characteristic length scale, and let ν be the kinematic viscosity of the fluid. The dimensionless Reynolds number is defined as $R = VH/\nu$, where H is the step height. We take a channel width W of two step heights H, where $H = 0.5$. We give incoming boundary conditions one channel width upstream of the step along the segment $x = -1.$, $0.5 \leqslant y \leqslant 1$, where the origin of the coordinate system is at the lower left corner of the channel (see Fig. 1). At the entrance, we assume a uniform entrance profile $(u, v) = (1, 0)$. It is important to discuss the choice of this inlet velocity profile. From the point of view of comparison with physical experiments,

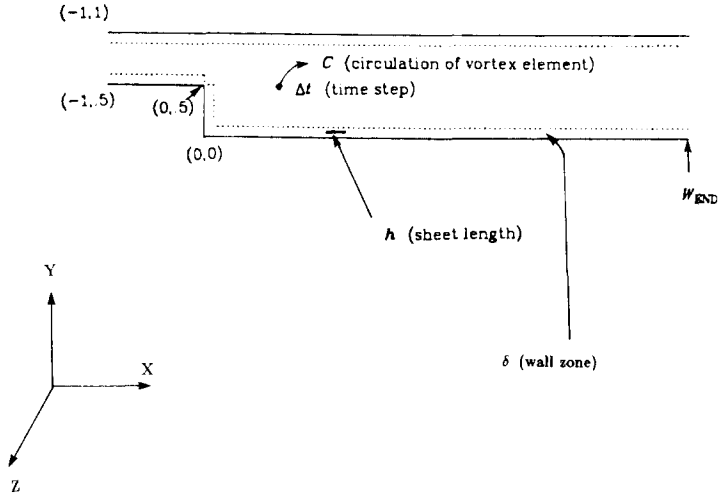

FIG. 1. Numerical parameters.

this entrance profile is uncommon; at low Reynolds number, a parabolic profile will develop in most experimental apparatus in the entrance section upstream of the step. In fact, we do satisfy the no-slip condition between the line $x = -1$ (channel entrance) and $x = 0$ (edge of the step). Thus the flow will neither be uniform when it reaches the edge of the step, nor will it be fully developed Poiseuille flow over such a short distance, and this will be a source of disagreement between our calculations and experiment.

There are two reasons why we chose this uniform entrance profile. Our goal is to focus on the effect on the solution of changing numerical parameters. First, by assuming a uniform entrance profile, all vorticity in the flow comes from the no-slip condition along the wall, and the numerical parameters involved in the creation of vortex sheets are the sole factors in determining the total number of vortex elements (sheets and blobs). A parabolic entrance profile would require a discretization of the entrance vorticity distribution into vortex sheets and blobs; we wished to limit the manner in which vorticity is created. Second, we wish to run experiments over a wide range of Reynolds numbers. A parabolic inlet profile depends on the Reynolds number. In the vortex method, the only manifestation of the Reynolds number is in the size of the random step taken in the solution of the diffusion equation; we want to study the eddy structure of the solution as the balance between advection and diffusion changes, always maintaining the same boundary conditions. We point out, however, that is a simple matter to integrate a given inlet profile into the vortex method if one so defines.

The numerical parameters are linked as follows. As input, we supply the time step Δt, the sheet length h, the circulation C of an individual vortex element, and the length of the channel downstream of the step W_{END} (see Fig. 1). Vortex sheets are created at points spread a distance h along the wall. Since the circulation $C =$

$h \cdot (\xi_{\max})$, halving C with h fixed doubles the number of vortex sheets; cutting h in half with C fixed creates half as many doubly strong sheets at twice as many points. The time step Δt is a particularly intricate parameter, since it controls (a) the size of the time step used in the time integration of the advection equation, (b) the size of the random step, (c) the size of the numerical boundary zone δ, and (d) how often the no-slip condition is satisfied. In addition, the scaling σ of the smoothing function f is related to h by $\sigma = h/\pi$ (see [22, 42]); thus the "singularity" of an individual vortex blob is controlled by the discretization of vorticity along the wall. We will not change the smoothing function itself, and shall use the smoothed structure given in [10], resulting in a stream function for a single vortex blob of circulation C of

$$\Psi(r) = \begin{cases} (-C/(2\pi))\log(r) & r \geqslant \sigma \\ (-C/(2\pi))((r)/\sigma + \log(\sigma) - 1) & r < \sigma \end{cases}. \tag{4}$$

V. Comparison of Calculated Results with Experiment

In this section we compare the results of our most refined calculations with available experimental data. There are a large number of ways to define the Reynolds number $R = VL/\nu$: some choices for L have been the step height, the channel height, inlet height, and the hydraulic diameter; for the characteristic speed, investigators have used the maximum inlet velocity, the average inlet velocity assuming a parabolic profile, and the speed at which the apparatus is towed through the fluid. To normalize the various experiments, we instead use the classification given in [3] of the three ranges of separated flow: (1) laminar flow, in which the flow is laminar from the separation off the step all the way beyond reattachment, (2) transitional flow, which is laminar at the separation point but becomes turbulent prior to reattachment, and (3) turbulent flow, in which the boundary layer is turbulent prior to separation.

A1. *Laminar Flow-Experimental Results*

In the laminar regime, the flow structure is characterized by a single, elliptically shaped recirculation zone [3, 13, 19, 25, 32, 37]. The flow is essentially two-dimensional; Armaly *et al.* [3] found a 1% spatial variation in the downstream velocity in the spanwise z direction (time variation is discussed below). Denham and Patrick [13], found a less than 2% spatial variation in the total flow rate in the x direction along the center plane, indicating that the flow was self-contained along that plane.

The flow is reasonably stable and steady. Kueny and Binder [28] report that velocity at a fixed point did not vary by more that 1% in time in their experimental apparatus. At the low and medium Reynolds numbers within the laminar regime, Denham and Patrick [13] report that if the apparatus is tapped, velocities within the main flow return to original values, while velocities near the reattachment point settle to new values which differ from the old by less than 1% of the average

channel velocity; indicating "that a small range of semi-stable recirculation zone configurations exist at each Reynolds number." This is an important point, since we are using a probabilistic technique to compute the solution to a problem that eveidently contains a range of stable solutions. (Note that some numerical schemes for viscous flow over a backwards step assume the solution is time-independent [3, 8, 21, 32, 37] and compute the solution by iteration.) At the high end of the laminar regime, time fluctuations in the reattachment point appear, and bending of streamlines along the top wall opposite the reattachment point occurs, indicating the onset of the transitional regime [13].

Honji [25] reports that the elliptical structure develops continuously from potential flow for impulsively started flow over a step without a wall. The reattachment length x_l for laminar internal flow scales with the step height H, yielding a normalized reattachment length $x_R = x_l/H$ which increases linearly [19] with Reynolds number [3, 13, 19, 25, 28] until the laminar quality of the flow breaks down. The center of the reattachment eddy ("normalized eddy center") remains nearly constant when normalized with respect to the reattachment length, with coordinates $(x_C, y_C) = (0.3x_R, 0.6H)$, indicating [13] that laminar flow is essentially self-similar in that experimental values for the normalized reattachment length for different Reynolds numbers lie on a single curve, and the normalized eddy center remains fixed.

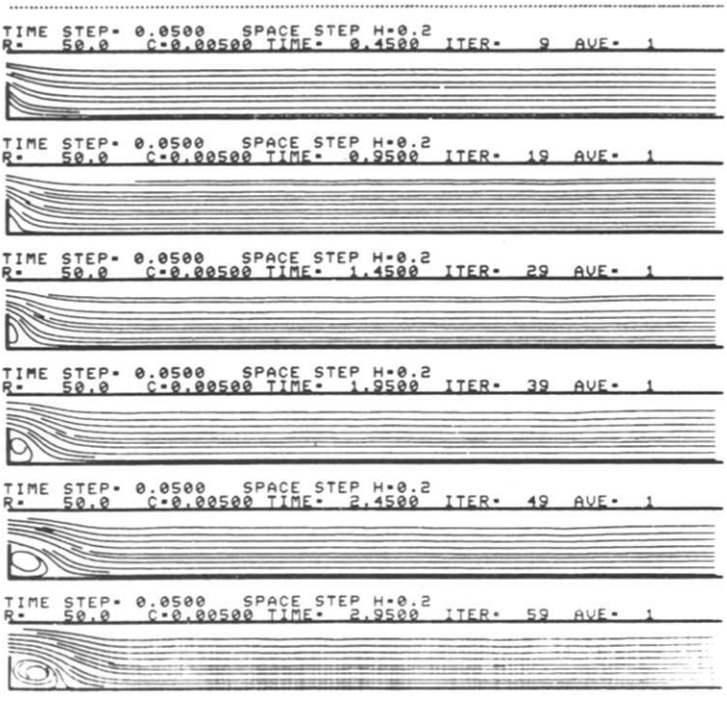

FIG. 2. Startup of flow, $R = 50$.

A2. *Laminar Flow-Numerical Results*

We begin with the results of a calculation performed with $R = 50$, $h = 0.2$, $\Delta t = 0.05$, $C = 0.005$, and $W_{END} = 10$ (exit 20 step heights downstream). In Fig. 2, we show the startup from a potential flow as the no-slip condition is instantaneously imposed at $t = 0$. We show "instantaneous streamlines" every 10 time steps, obtained as follows (the data is not time-averaged). The velocity at each point of a uniform (10×100) grid is calculated from the positions and strengths of vortex elements. Using this fixed discrete velocity field, the trajectory of a particle started within each grid cell is drawn, providing the "instantaneous streamlines." The recirculation bubble develops smoothly from the potential flow, in agreement with the experiments discussed earlier. In Fig. 3a, we show successive time portraits of the long-time behavior for $R = 50$ and in Fig. 3b for $R = 125$ (numerical parameters are unchanged). Here, as observed experimentally, there is a single, elliptical recirculation zone with downstream reattachment to the bottom wall. The bubble is essentially steady, although definite oscillations are seen in these calculations; the size of the variation in the computed shape depends on the number

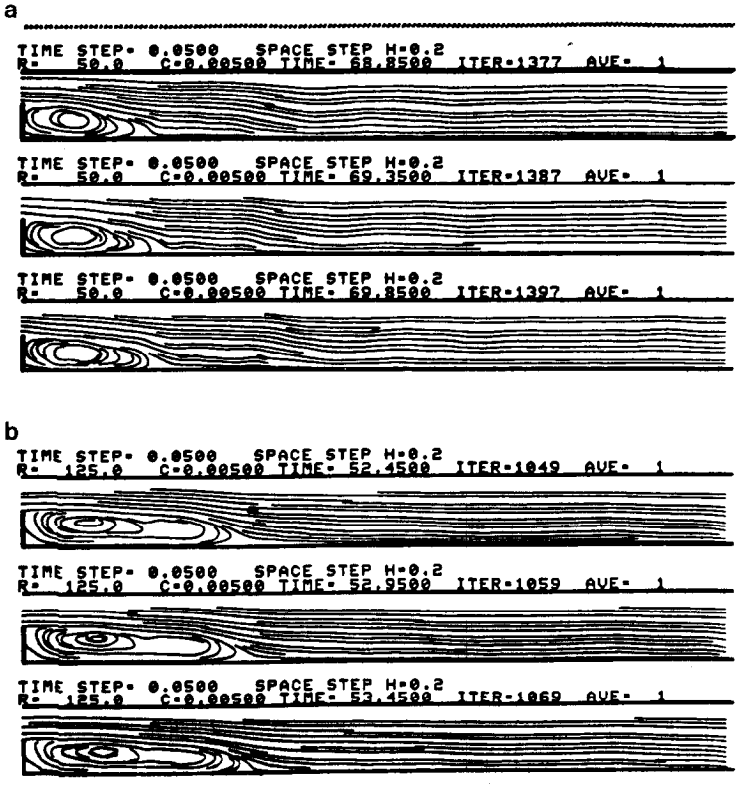

FIG. 3. Successive time portraits of fully developed flow, (a) $R = 50$; (b) $R = 125$.

N of vortex elements, and decreases as N is increased (see section on convergence). This is a delicate point: since experimental results indicate a small range of semi-stable solutions and we are constantly perturbing the flow through our random walk solution to the diffusion equation, it is not clear that the time variation in our calcuations should necessarily vanish as N goes to infinity. For the given value of N, however, the oscillation shown is clearly due to the response of the solution to a high level of noise in the random walk. When the flow is averaged over 2000 time steps, the normalized reattachment length is $x_R = 1.7$ for $R = 50$ with calculated eddy center at $(0.59, 0.29) = (0.34x_R, 0.59H)$; for $R = 125$, $x_R = 3.1$ and the eddy center is at $(1.0, 0.31) = (0.32x_R, 0.62H)$, both in excellent agreement with the self-similar value of $(0.3x_R, 0.6H)$ reported in Denham and Patrick [13].

B1. *Transitional and Turbulent Flow-Experimental Results*

The transitional stage is marked by the collapse of the two-dimensional, single recirculation eddy, stable picture of the flow. As the Reynolds number is increased, the flow becomes three-dimensional [3], as indicated by checking spanwise velocity profiles at various points downstream, however, symmetry about the center plane is maintained. The central feature of three-dimensionality in the transition regime is the presence of longitudinal (spanwise) vortices which are responsible for dissipating structures in the flow [3]; these structures are most pronounced in the middle of the transition range, and drop out and disappear as the flow becomes turbulent. Laminar flow separates from the step and becomes unsteady midway to the reattachment point [14]. Fluid is entrained by the recirculation bubble, and eddies detach and move downstream as large three-dimensional eddies [3, 7, 13, 14, 19, 25] whose cross sections vary in the spanwise direction [3]. For flow without a top wall [7, 16, 25], the flow splits at reattachment, with the large recirculation eddy torn into two; part of the flow goes upstream into the recirculation zone to supply the entrainment and part of the eddy is shed downstream, suffering a decrease in eddy length scale.

For step flow with a confining upper wall, there is a continuous mechanism of (1) fluid entrainment by a growing recirculation zone, (2) detachment of eddies which move downstream resulting in (3) a smaller recirculation zone which then entrains more fluid. The large eddies move downstream and cause local flow reversal, as observed in [3, 14, 15, 19, 26]. Durst and Tropea [14] report that in the transitional regime, streamlines are wavy right after the step, and break into "vortex rolls" after 3–4 step heights downstream; as R increases, vortex formation occurs further and further upstream. Eaton and Johson [15] characterize them as "large, turbulent, spanwise eddies" which effect large local flow reversal. These three-dimensional eddies are responsible for dissipating structures and coupling together the various recirculation regions [3].

Unlike laminar flow, increasing the Reynolds number for transitional flow brings a decrease in the mean reattachment length, defined to be the point along the bottom wall where the time averaged mean velocity field is zero. The averaging period required in order to obtain acceptably small variance of the mean can be quite long

(see [3, 14, 26]). Instantaneous measurements [14, 26] show the reattachment point moving backwards and forwards as large eddies pass by over a distance along the bottom wall of as much as four step heights [14]; local intermittent flow reversal is observed to occur well outside this range [1, 26]. The mean reattachment length decreases with increasing Reynolds number to a local minimum, at which point the shed vortices are largest [3, 14].

Along the top wall, the bending streamlines now form a full new separation zone containing fluid recirculating in the opposite direction as that within the main bubble. This top wall eddy persists throughout the transition regime and appears due to an adverse pressure gradient created by the sudden step expansion [3]. This downstream moving eddy is reported by a number of observers; time-averaged streamline plots [3, 14, 26] show a recirculation eddy whose position moves upstream along the top wall with increasing Reynolds number. Finally, a small, clockwise rotating recirculation eddy located at the base of the step between the corner and the large eddy is observe [3, 7, 28, 36].

The local minimum in mean reattachment length as R signals the end of the transition regime and the beginning of turbulent flow. As R increases, the mean reattachment length quickly grows to about 6–8 step heights and remains constant from then on [3, 14, 19, 26, 36]: additional references are provided in [19]. As R increases into the turbulent regime, the eddies shed off the recirculation bubble decrease in size until they finally disappear [3, 14, 36], paralleled by an increase in turbulent mixing [14] and a return to an essentially two-dimensional flow [3].

B2. *Transitional and Turbulent Flow—Numerical Results*

In Fig. 4, we show the results of a calculation with $R = 500$, well into the transitional regime, with $\Delta t = 0.5$, $C = 0.025$, $h = 0.2$, and $W_{\text{END}} = 10$. The flow picture has radically changed; large eddies are shed off the recirculation bubble and progress downstream as distinct structures which decay in size, in agreement with the experiments described earlier. Once these eddies break away, they move with very close to constant speed $\frac{1}{2}$, where the inlet speed is unity. This was calculated in two ways, first, by drawing a line through the center of a particular moving eddy in the successive time drawings, and second, by placing a moving time window over a given eddy and finding the reference frame speed which minimized motion of the center. Computer-generated movies show that the velocity of this large eddy is quite different from the velocities of the defining particles; individual particles move in and out of the moving eddy, similar to the distinction between group wave velocity and individual fluid particle motion. The calculation at $R = 500$ was carried out for 30 times longer than the time window shown (i.e., 2500 time steps, counting startup), with 13 separate eddies exiting the channel during that time, an average rate of 1 eddy every 7.9 time units. In Fig. 5, we stand at the point (8.0, y), which is 80% of the distance down the channel from the step and plot the u velocity as a function of time and height, showing the fixed frequency of eddy shedding. The changes of sign in u indicating the passage of an eddy are more pronounced near the top and bottom walls (away from the middle).

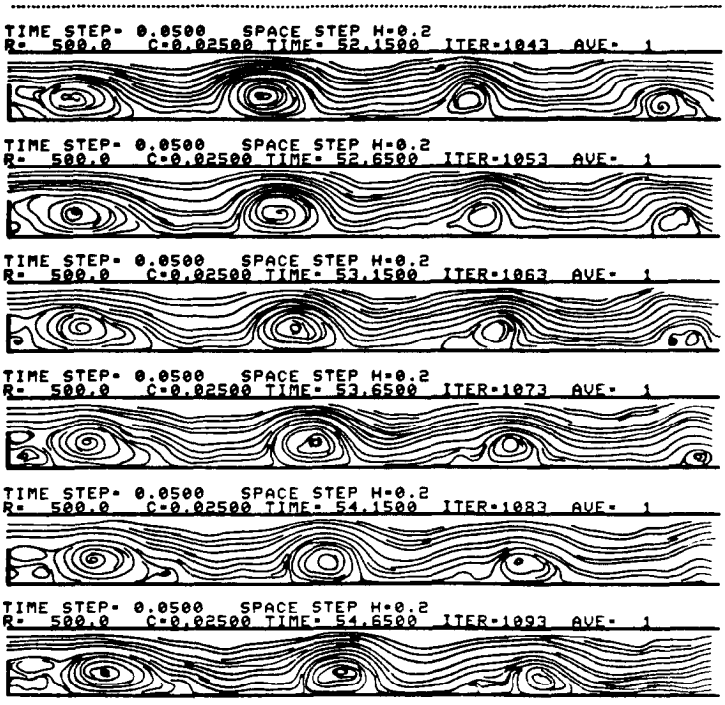

FIG. 4. Successive time portraits of fully developed flow, $R = 500$.

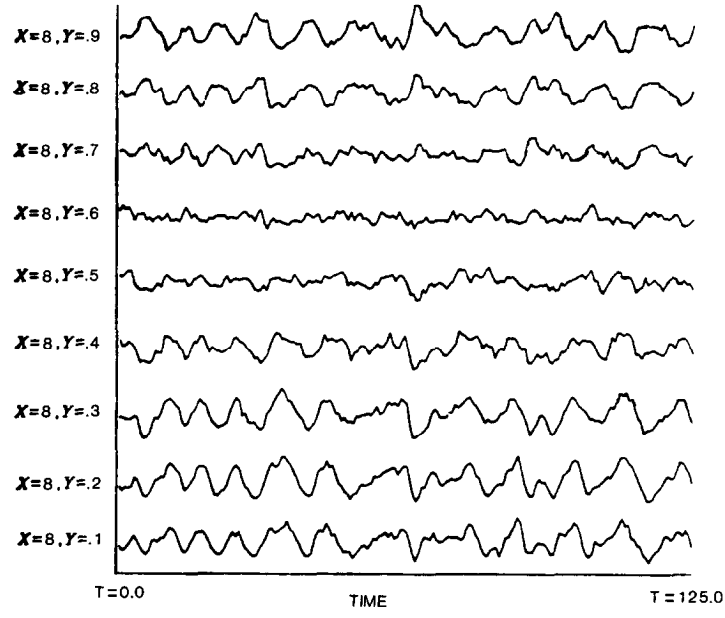

FIG. 5. U velocity plotted against time, $R = 500$; station at $X = 8.0$.

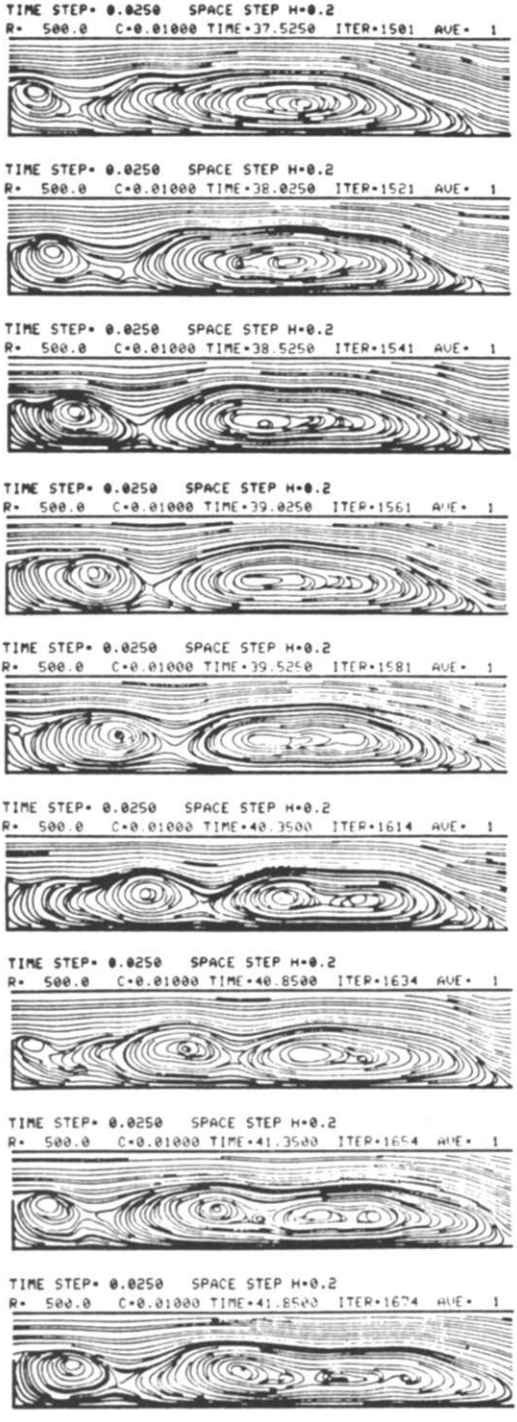

FIG. 6. Blow-up of corner for $R = 500$.

With numerical parameters unchanged, we repeated the above calculation with $R = 375$ and $R = 250$, more towards the lower end of the transitional regime. While eddies continue to break away from the recirculation bubble, they rapidly dissipate

eddies decreases with decreasing R until the laminar, single recirculation bubble picture is reached. At both $R = 375$ and $R = 250$, the large eddy velocity is constant at $\frac{1}{2}$, and the shedding frequency (number of eddies/time) is 9.8 for $R = 375$ and 9.4 for $R = 250$.

Returning to the flow portrait at $R = 500$, our computed solution differs from experimental observations in two ways. First, in the real flow, the shed vortices are spanwise three-dimensional structures. While we believe that our computed eddies are a legitimate part of the solution to the two-dimensional equations, the vorticity stretching term in the three-dimensional equations allows these structures to dissipate in the spanwise direction and our 2D eddies persist longer than should be observed. Second, most experiments describe a recirculation eddy that oscillates and is torn in two by the incoming flow; the shed eddy moves downstream and another eddy forms and grows by entraining more fluid as the process repeats itself. In the calculation shown, the new recirculation eddy is quite small, probably

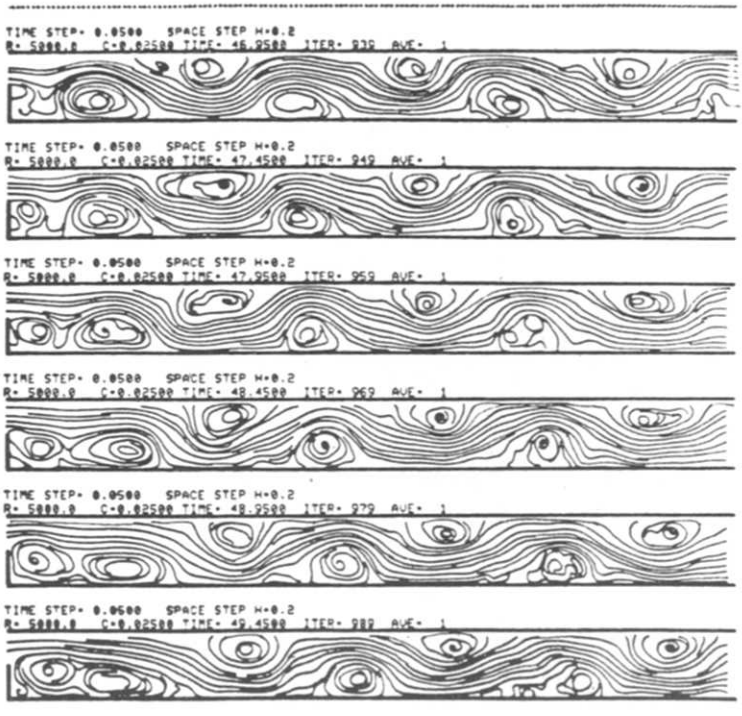

FIG. 7. Successive time portraits of fully developed flow, $R = 5000$.

because we did not use enough vortices to adequately resolve this detailed mechanism. To address this issue, we repeated the calculation with $C = 0.01$, $\Delta t = 0.025$, and $h = 0.2$, producing approximately 2.5 times as many vortices. Successive time portraits of this calculation as shown in Fig. 6, demonstrating that the oscillating recirculation bubble is stretched and distorted by the incoming flow, and this tears away the downstream end of the bubble.

In Fig. 7 we show the results of a calculation at $R = 5000$, in the "two-dimensional turbulent" regime, with $\Delta t = 0.05$, $h = 0.2$, $C = 0.05$ and $W_{\text{END}} = 10$. The bending of streamlines seen earlier at about 3–4 step heights downstream has now turned into separation along the top wall, and counterrotating eddies are shed which interlace with eddies shed from the recirculation bubble. In Fig. 8, we show long time-averaged streamlines plots at $R = 50$, $R = 125$, $R = 250$, $R = 375$, $R = 500$, and $R = 5000$, and in Fig. 9 we plot reattachment length as a function of Reynolds number. As seen in experiment, the reattachment length grows approximately linearly, reaches a maximum somewhere between $R = 250$ and $R = 375$, and then falls back down. At $R = 250$, the eddy center is at $(1.89, 0.31) = (0.44x_R, 0.62H)$, at $R = 375$ at $(1.59, 0.32) = (0.38x_R, 0.64H)$, at $R = 500$ at $(2.11, 0.29) = (0.53x_R, 0.58H)$, and at $R = 5000$ at $(1.8, 0.3) = (0.66x_R, 0.6H)$, showing the breakdown in the self-similar nature of the time-averaged flow at the higher Reynolds numbers. In the time-averaged plots for $R = 375$, $R = 500$, and $R = 5000$,

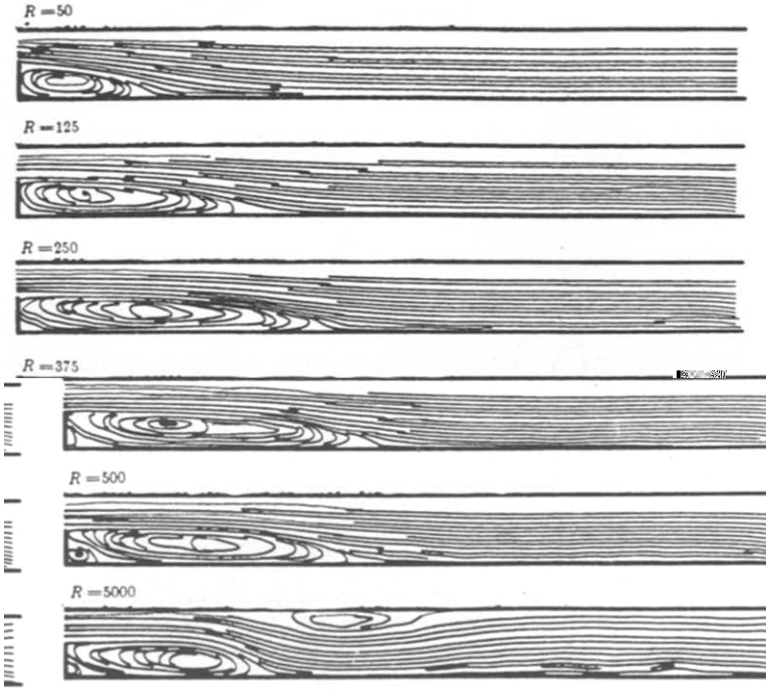

FIG. 8. Averaged streamlines over 2000 time steps.

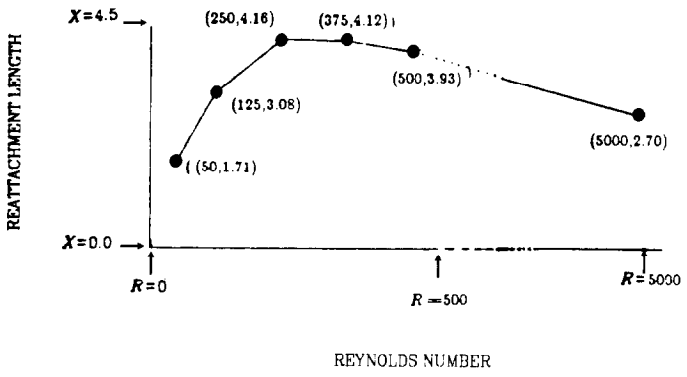

FIG. 9. Reattachment length as a function of Reynolds number, $R = 50, 125, 250, 375, 500, 5000$.

the counter-rotating eddy in the lower left corner is seen. Finally, along the top wall at $R = 5000$, we see the fixed position of the counterrotating separation eddy reported in [3, 14, 26]. The center of this eddy is at (4.1, 0.9) (8 step heights downstream), indicating that we are well into the "turbulent" regime.

VI. Dependence of Solution on Numerical Parameters

A. *Laminar Flow*

We analyze the dependence of the computed solution on numerical parameters at $R = 50$ where the fully developed real flow is essentially time-independent (steady). We analyze convergence under a variety of measures, from highly integrated statistics to pointwise, instantaneous quantities.

In Fig. 10a, we plot the total circulation $\Gamma(t)$ for various values of C, calculated by summing the circulation of all the vortex elements at time t (other numerical parameters are held fixed). As C is decreased, the number N of vortex elements increases. The calculation runs from $t = 0$ (start up) to $t = 50.0$, which corresponds to 1000 time steps. The number of vortex blobs A and total number of vortex elements B (sheets plus blobs) is shown in the figure as (A, B). Long-time behavior has set in after about 200 time steps. Let $\bar{\Gamma}$ be the average value of $\Gamma(t)$ over time steps 200 to 1000. We observe that (i) the oscillation of $\Gamma(t)$ around $\bar{\Gamma}$ decreases as N increases and (ii) $\bar{\Gamma}$ stays relatively fixed as N increases, showing convergence of the means as N increases. To establish a convergence rate, in Fig. 10b we plot the variance $\frac{1}{500}\sum_{n=500}^{1000} |\Gamma(n\,\Delta t) - \bar{\Gamma}|^2$ against the number of vortices. The graph roughly corresponds to a convergence rate of order $1/N$: halving the circulation of the individual vortex elements halves the variance in the solution.

In Fig. 11a, we hold (h, C, W_{END}) fixed and decrease Δt by a factor of 2. The variance in $\Gamma(t)$ around $\bar{\Gamma}$ is about the same in both plots [7% for $\Delta t = 0.05$ and 8% for $\Delta t = 0.025$], and the mean $\bar{\Gamma}$ is virtually unchanged: $\bar{\Gamma} = 0.36$ for $\Delta t = 0.05$

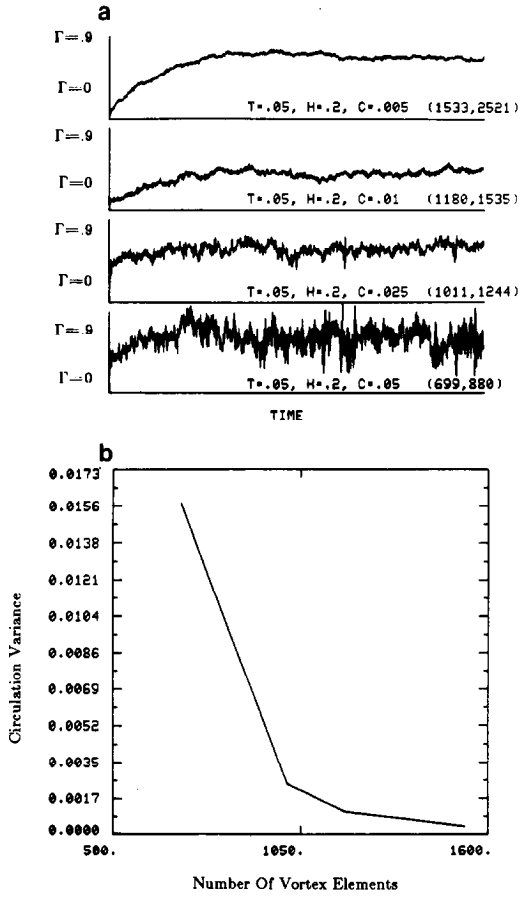

FIG. 10. (a) Total circulation vs time. (b) Decay of circulation variance as a function of number of vortices.

and $\bar{\Gamma} = 0.31$ for $\Delta t = 0.025$. Note the additional number of vortex elements resulting from the smaller time step. These results indicate that, at low Reynolds number, the large jumps in positions of the vortices to approximate the diffusion equation dominate any increase in accuracy associated with better time integration along the particle trajectories. Thus, the numerical diffusion error associated with advecting the particles (see [42]) is overshadowed by the actual physical viscosity. In Fig. 11b, we hold $(\Delta t, C, W_{\text{END}})$ fixed and halve h, the sheet length, decreasing the core size. For a steady flow with a single reattachment point, little difference can be seen in the two plots (variance is 8.4% for $h = 0.2$, and 8.5% for $h = 0.1$, and the $\bar{\Gamma}$ is 0.52 for $h = 0.2$ and 0.56 for $h = 0.1$).

These results indicate that C is the most important parameter controlling accuracy for this range of flow. This is reasonable, since at low Reynolds number,

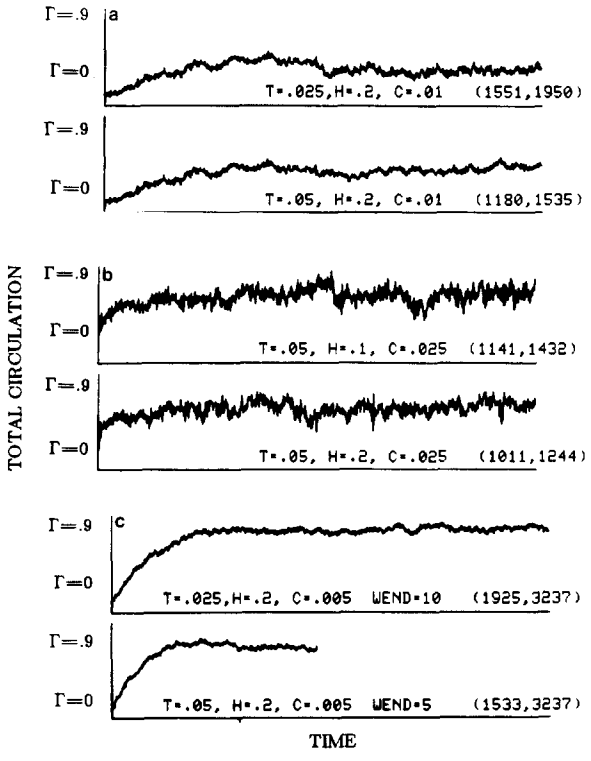

FIG. 11. Total criculation vs time.

the physical diffusion term is large and more vortex elements reduce the noise in the random walk solution to the diffusion equation. We check two other parameters: the dependence of the solution on the particular random number string chosen (the initializing seed) and the length of the truncated channel. In Fig. 11c, we hold $(\Delta t, h, C)$ fixed, double the channel length, and start with a different seed in the random jump subroutine. The variance is 3.5% ($\bar{\Gamma}=0.61$) for $W_{\text{END}}=5$ and 4.0% ($\bar{\Gamma}=0.62$) for $W_{\text{END}}=10$, indicating that results are essentially independent of starting seed and that $W_{\text{END}}=5$ is long enough for this calculation.

The total circulation is a global quantity of the flow. The next level of sensitivity is to analyze the velocity field. Since we are dealing with a Lagrangian method, we compute $\mathbf{u}_{ij}^n$, where $\mathbf{u}_{ij}^n$ is the velocity on a uniform rectangular grid at time step $n\,\Delta t$ at the point $i\,\Delta x$, $j\,\Delta y$, and $\Delta x=\Delta y=0.1$, $0\leqslant i\,\Delta x\leqslant W_{\text{END}}$, $0\leqslant j\,\Delta y\leqslant 1$. We first study time averaging as a technique for removing "noise," i.e., time variation around the mean, in the solution. Let $\mathbf{u}_{ij}^n(M)$ be the velocity field obtained by averaging $\mathbf{u}_{i,j}^n$ over M time steps. Let $\text{Err}(M)$ be defined as

$$\text{Err}(M)=\frac{1}{W(M)}\sum_{\text{windows of length}}\left(\frac{1}{I\cdot J}\sum_{i,j}|\mathbf{u}_{i,j}^n(M)-\mathbf{u}_{i,j}^n(500)|^2\right)(|\mathbf{u}_{i,j}^{(5000)}|^2)),$$

where $W(M)$ is the number of windows of length M and $I(J)$ is the total number of points in the $x(y)$ direction. In other words, $\mathrm{Err}(M)$ is the average relative L^2 error in the discrete velocity field between a time average portrait of length M steps and the time average portrait of length 500 steps (all averages start at time step $n = 500$, thus $M = 500$ corresponds to averaging over time steps 500 to 1000). In Fig. 12, this quantity is plotted against M, the size of the sample window. Here, the average is taken over all "windows" of length M, and the norm $|\mathbf{u}| = (u^2 + v^2)^{1/2}$. For example, for $M = 2$, we calculate the average relative L^2 error between velocity fields obtained from averaging over 2 time steps and the velocity field obtained from an averaging window 500 time steps long. The results indicate that the more the numerical parameters are refined, the more the short-time average velocity field

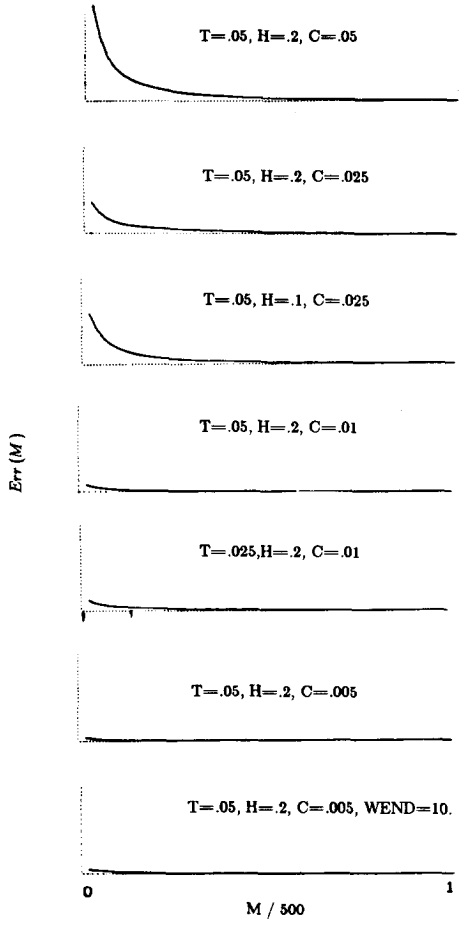

FIG. 12. Error $\mathrm{Err}(M)$ in velocity between averaging window of size M vs full average: $\mathrm{Err}(M) = (1/(M)(W(M)) \sum_{\text{windows of lengh } M} ((1/I \cdot J) \sum_{i,j} |\mathbf{u}^n_{i,j}(M) - \mathbf{u}^n_{i,j}(500)|^2)/(|\mathbf{u}^n_{i,j}(500)|^2)$ (sample window size)/(maximum window size) $= M/500$.

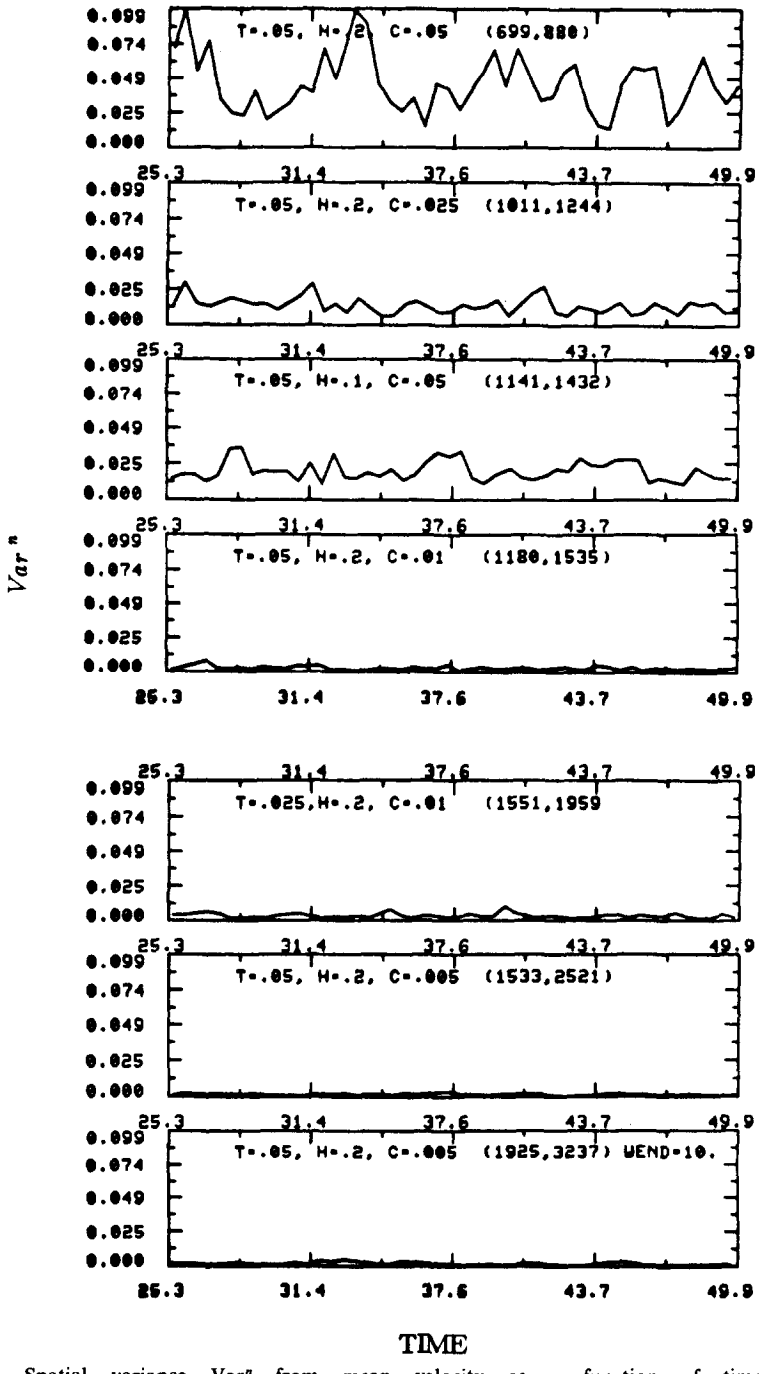

FIG. 13. Spatial variance Var^n from mean velocity as a function of time: Var^n $(1/(I \cdot J)) \sum_{i,j} |\mathbf{u}_{i,j}^n - \bar{u}_{i,j}|^2$.

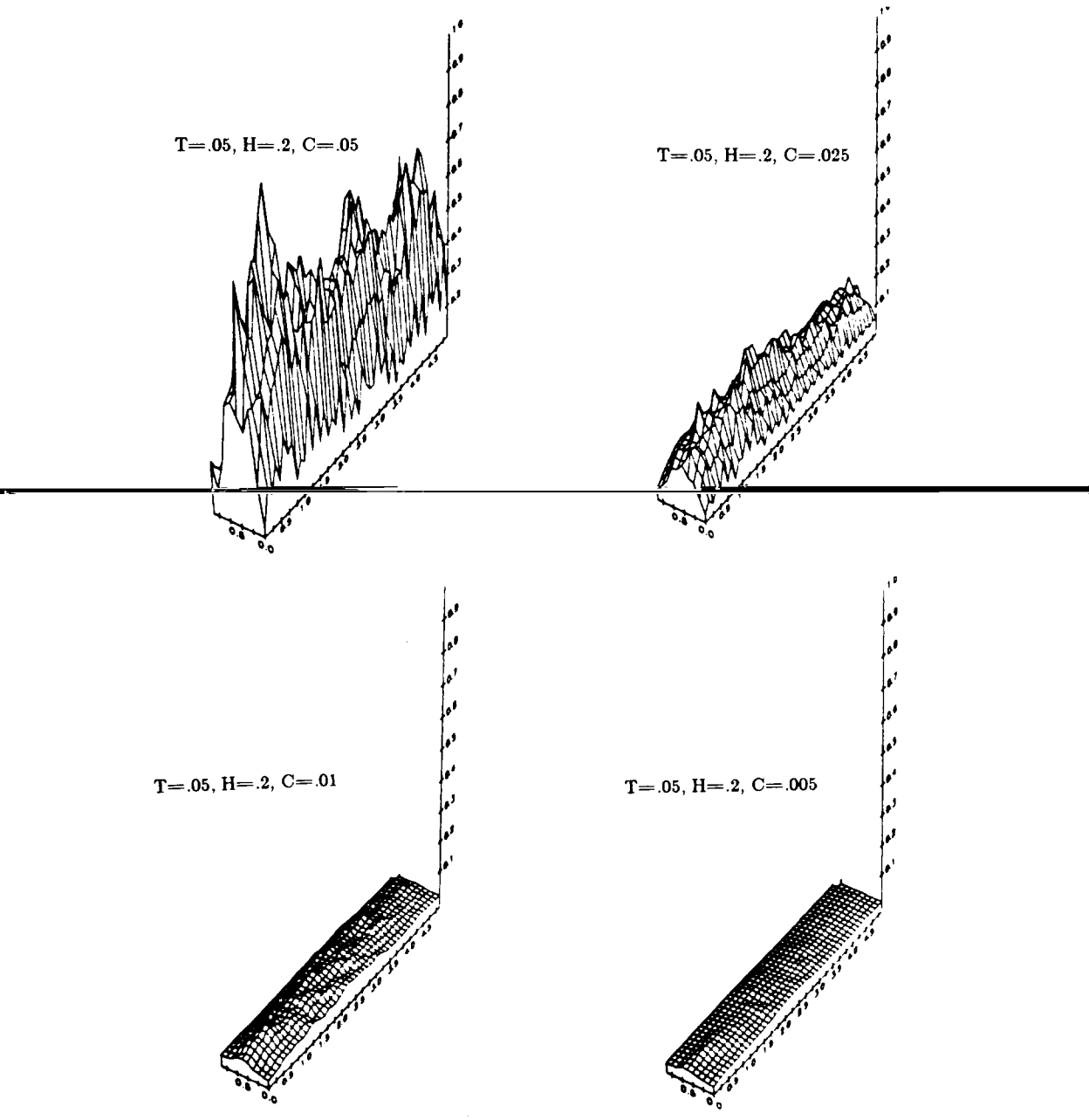

FIG. 14. Temporal variance $\mathrm{Var}_{i,j}$ from mean as a function of space: $\mathrm{Var}_{i,j} = \frac{1}{500}\sum_{n=500}^{1000} |\mathbf{u}_{i,j}^n - \bar{u}_{i,j}|^2$ (graphs normalized so the maximum height over all surfaces is unity).

looks like the long-time average field; the dropoff for each curve is like $1/M$. Note once again that changing C reduces the variance the most.

Let $\bar{u}_{i,j}$ be the velocity field obtained by averaging over time steps 500 to 1000. Then $\text{Var}^n = (1/(I \cdot J)) \sum_{i,j} |\mathbf{u}^n_{i,j} - \bar{u}_{i,j}|^2$ is the spatial variance at time $n\,\Delta t$ of the instantaneous field from the mean. In Fig. 13, we plot Var^n as a function of time, showing that as numerical parameters are refined, the instantaneous velocity field settles to the average velocity field. Again, changing C reduces the variance the most. A graph of the spatial variance averaged in time against the number of vortices showed a convergence rate of roughly $1/N$, in agreement with our earlier estimate.

Next, we compute the temporal variation as a function of space, that is, at each grid point i, j we compute $\text{Var}_{i,j} = \frac{1}{500} \sum_{n=500}^{n=1000} |\mathbf{u}^n_{i,j} - \bar{u}_{i,j}|^2$. We plot $\text{Var}_{i,j}$ as a surface in Fig. 14, showing that as the numerical parameters are refined, the temporal variance around the computed mean at each point decreases. In Fig. 15, we calculate $\text{Var}_{i,j}$ against the number of vortices at a variety of points in the domain. Two observations can be made. First, the curves are all roughly of the form $1/N$,

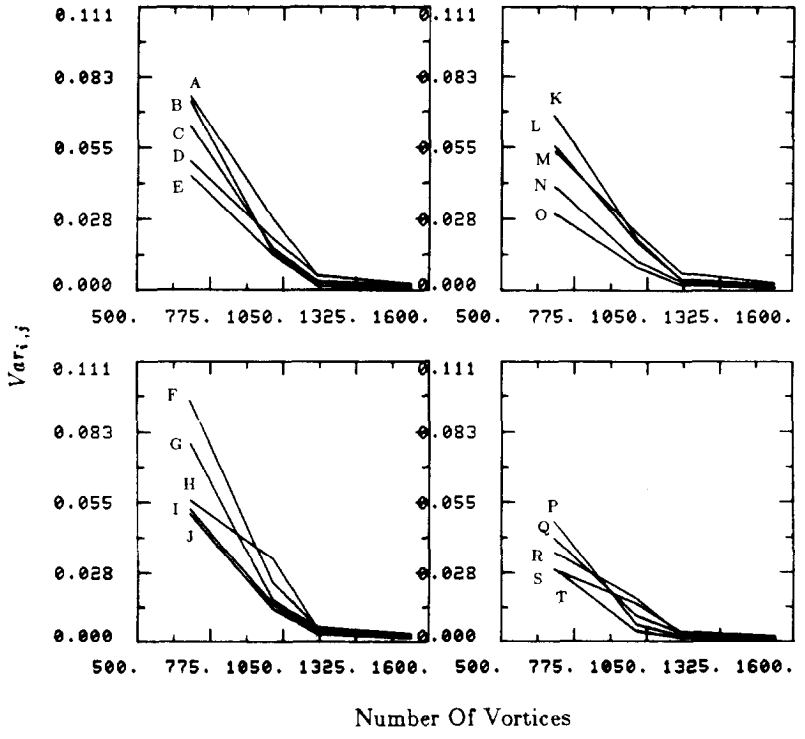

FIG. 15. Decay of temporal variance $\text{Var}_{i,j}$ from mean at select points i, j in domain: $A = (1., 2.)$, $B = (2., 2.)$, $C(3., 2.)$, $D = (4., 2.)$, $E = (5., 2.)$, $F = (1., 4.)$, $G = (2., 4.)$, $H = (3., 4.)$, $I = (4., 4.)$, $J = (5., 4.)$, $K = (1., 6.)$, $L = (2., 6.)$, $M = (3., 6.)$, $N = (4., 6.)$, $O = (5., 6.)$, $P = (1., 8.)$, $Q = (2., 8.)$, $R = (3., 8.)$, $S = (4., 8.)$, $T = (5., 8.)$.

showing no error between the finest calculation and itself. As expected, the means tend towards the limiting profile. Further calculations and error analysis are in [43].

Finally, we wish to establish a single point, instantaneous measurement. In Fig. 17, we plot the position of the reattachment point as a function of time for different numerical input parameters. The reattachment point is determined by starting at $(x=0.1,\ y=0.05)$ and moving in the positive x direction until the velocity changes sign. This is an extremely sensitive test for the vortex method, since the local instantaneous velocity field can change quite drastically if too few vortex elements are used to resolve the boundary layer. Note that the top three calculations are sufficiently crude that the location of this point jumps wildly during a single time step. However, as the parameters are refined, the variation in position settles down and the reattachment point is relatively constant for the finest calculation.

We can summarize the results as follows. For laminar flow, accuracy is controlled primarily by the number of vortex elements. The variance in the total circulation and the pointwise velocity from the mean decays as $1/N$, and the computed means

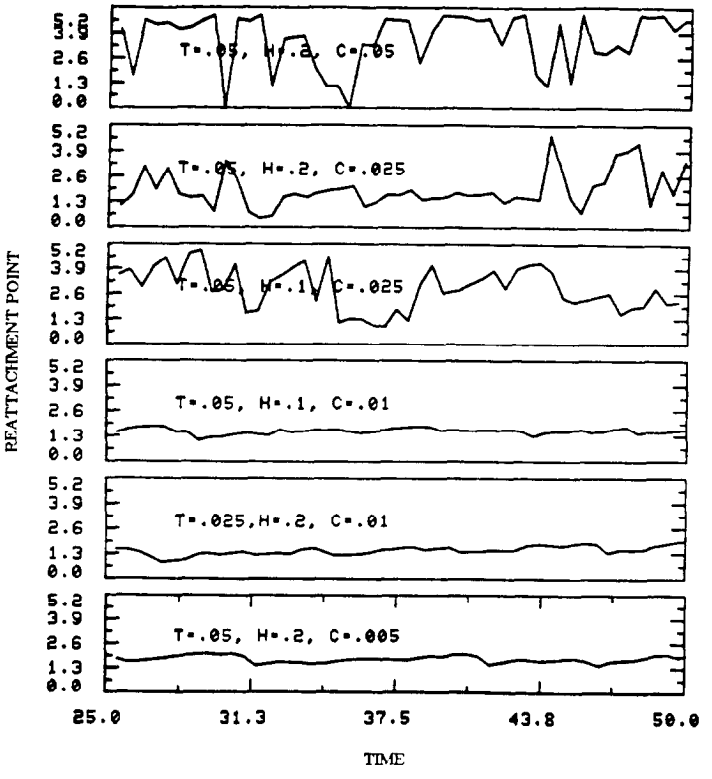

FIG. 17. Reattachment point vs time.

converge towards a limiting profile. Accuracy gained by refinement in Δt is overshadowed by the error in the approximation to the diffusion equation due to the large diffusive scale of the flow. Changing the sheet length, which also controls the smoothing radius of the vortex core, is of secondary importance. The effects of the changes in the numerical boundary layer, random seed and the truncation length are negligable.

B. *Transitional/Turbulent Flow*

At higher Reynolds number, the flow is no longer steady state and a periodic structure is seen. As shown earlier, large coherent vortex eddies detach from the separating shear layer and move downstream at a regular frequency. At this range of Reynolds numbers, the two-dimensional equations are unstable, and the instantaneous velocity at a particular point has little meaning. Energy combines at the smallest scales in an unpredictable manner, and it is only in the largest scales (coherent eddy structures) that one can see repeatability in a flow experiment. The typical response to this has been to analyze unsteady flow by measuring variations in flow quantities around means. While certainly a valuable approach, there are two problems. First, in both experiments and numerical computations, a very long time-averaging window may be required to gain reliable statistics independent of the window size; this was observed in several of the experiments cited. Second, in many engineering applications, the main goal may not be to find mean flow statistics. Instead, one is often interested in how large-scale structures develop, the stresses they exert on the body, and how they affect mixing within the flow. Thus, it is important to analyze the flow on some level between instantaneous measurements, which have little meaning, and long-time averaged statistics, which remove periodic dynamics. Our goal is to study the effect of refining numerical parameters on the computed large eddy dynamics.

We performed calcuations at $R = 500$, well outside the laminar regime. In order to make the computations affordable, we chose $W_{\text{END}} = 5$. Calculations were performed for all combinations $C = 0.05$, 0.025, 0.01, $\Delta t = 0.05$, 0.025, and $h = 0.2$, 0.1 (12 total runs), each running 500 time steps (1000 for $\Delta t = 0.025$) to become fully developed and then from 500 to 1000 (1000 to 2000 for $\Delta t = 0.025$) to provide data. In addition, an extremely long time (3000 time steps), extended channel ($W_{\text{END}} = 10$), refined ($C = 0.015$, $h = 0.2$, $\Delta t = 0.05$) calculation was performed, providing a large sample set from which to perform statistics and compare with the shorter time/shorter channel runs. This data set allowed us to check that the results obtained for the other runs did not depend on the channel length or time length of the computation.

We begin by studying the change in the large-scale structure of the flow as numerical parameters are refined. In Fig. 18, we show 6 successive time instantaneous streamlines of a calculation for $C = 0.05$, 0.025, 0.01, $\Delta t = 0.05$, $h = 0.2$. For $C = 0.05$, Fig. 18a ($N_{\text{TOT}} =$ total number of vortex elements at end of calculation $= 593$), the eddies are distinct structures which move downstream separately. For $C = 0.025$, Fig. 18b ($N_{\text{TOT}} = 865$), the same general picture is

presented, with smoother contours around the eddies. For $C = 0.05$, a typical downstream eddy consists of roughly 120 vortices, as compared with 210 for $C = 0.025$. The structures for $C = 0.05$ have some spurious smaller eddies attached to the large downstream-shed eddies, and these smaller eddies are not present in the more refined ($C = 0.025$) calculation. We believe that the smaller eddies in the former are due to numerical effects, since they are made up to relatively few (≈ 10) strong vortex elements and disappear in the more refined calculation. Finally, the shed downstream eddies in the coarser ($C = 0.05$) calculation have less well-defined eddy centers (multiple centers, etc.) than do those for the case $C = 0.025$. This is

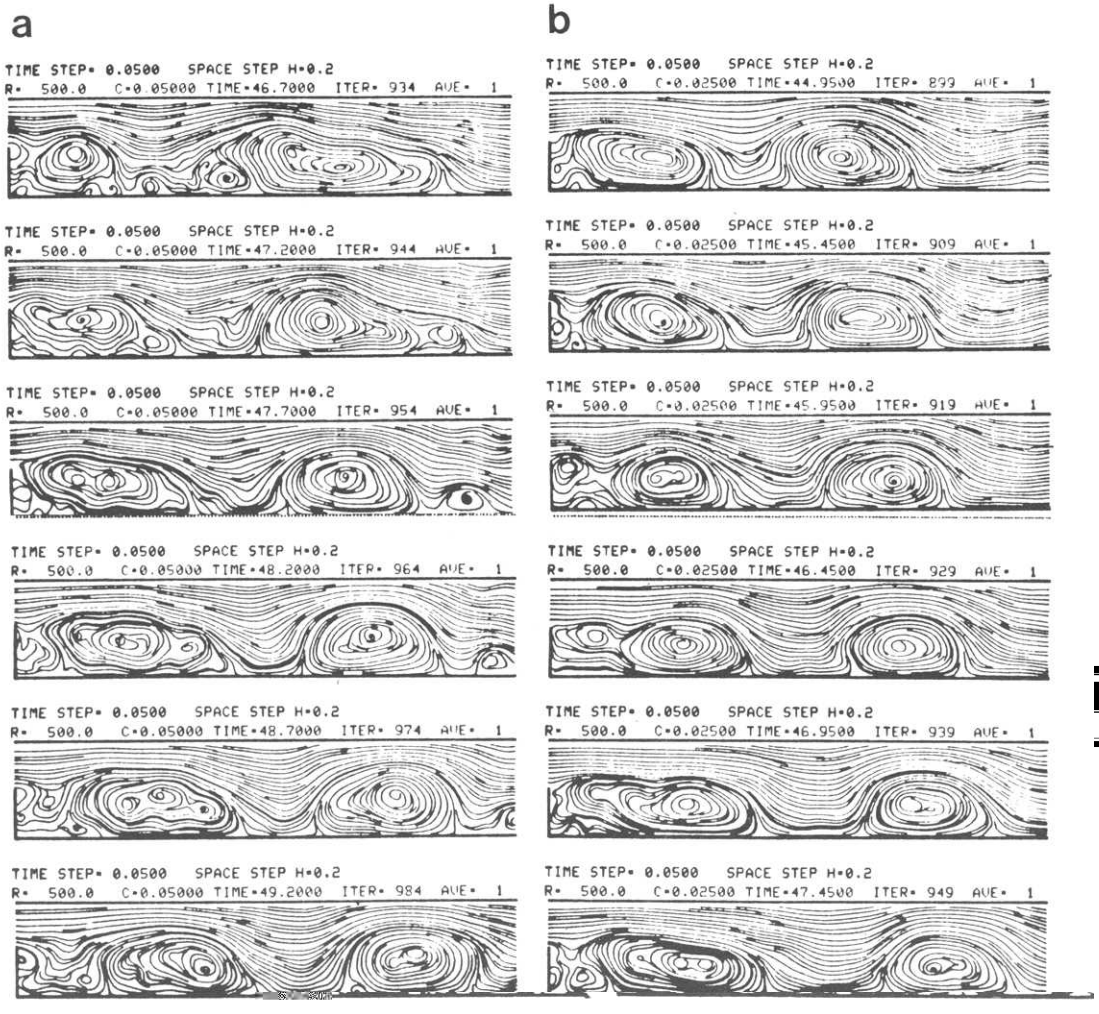

FIG. 18. Fully developed flow, $R = 500$; $C = 0.05$, 0.025, 0.01; $H = 0.2$; $\Delta t = 0.05$; $W_{\text{END}} \approx 5$.

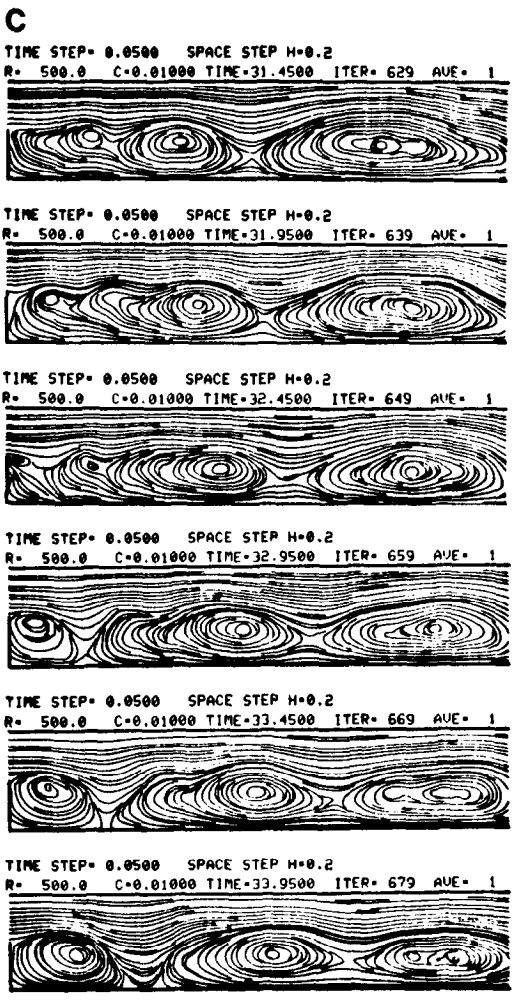

FIG. 18—*Continued.*

caused by using too few total vortex elements, which has the effect of creating artifical centers. These portraits are 5% of the total number computed, and their qualitative structure is representative of the full time calculations.

For $C = 0.01$, Fig. 18c, ($N_{TOT} = 1943$), this picture changes. Although the eddy centers are well defined, with few smaller spurious eddies, the boundaries between eddy structures blur. We hypothesized that this was due to a problem with the time step. At high Reynolds numbers, the size of the random step taken to approximate the diffusion equation is small compared to the error in the time integration scheme used for the advection step, in contrast to the low Reynolds number situation described earlier. When a large number of vortex elements are used to resolve the

boundary layer, many of them start off close together. Since the vortex method has an artificial diffusion error associated with time integration along particle trajectories (see [42]), with too large a time step the boundaries of the eddy structures diffuse and merge. The obvious test to check this hypothesis is to reduce the time step. First, however, we changed the sheet length h to make sure that the discretization of the no-slip condition was not the reason for this smearing of vortex structures. We performed calculations for $C = 0.05$, 0.025, and 0.01, $h = 0.1$ (sheets half as long) and $\Delta t = 0.05$. The same blurring occurred for $C = 0.01$. For the complete set of figures, see [43].

We then decreased the time step by a factor of 2 and repeated the above

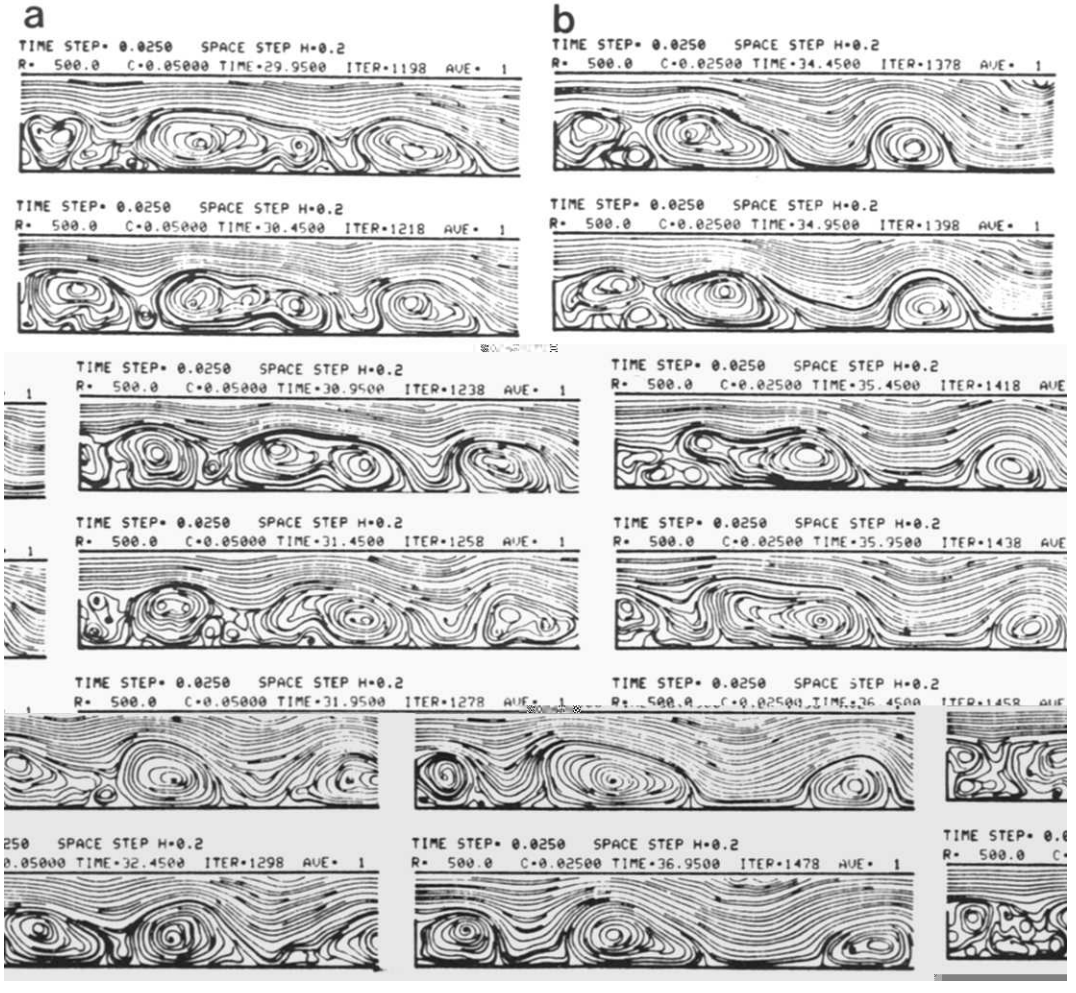

FIG. 19. Fully developed flow $R = 500$; $C = 0.05$, 0.025, 0.01; $H = 0.2$; $\Delta t = 0.025$, $W_{END} = 5$.

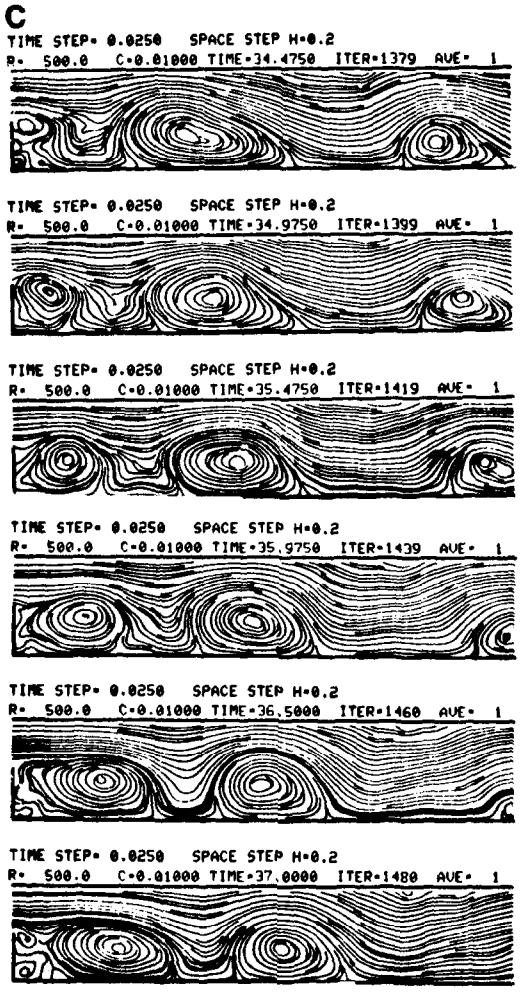

FIG. 19—*Continued.*

calculations. In Fig. 19, we show results for $C = 0.05$, 0.025, and 0.01, $h = 0.2$, and $\Delta t = 0.025$. In Fig. 19a, $C = 0.05$ ($N_{TOT} = 651$), we have distinct structures, but rough contours, spurious eddies and multiple centers. In Fig. 19b, $C = 0.025$ ($N_{TOT} = 1096$), contours are smoother, and eddy centers and boundaries are better defined. In Fig. 20c, $C = 0.01$ ($N_{TOT} = 2045$), contours are still smooth and centers and boundaries are well defined. Thus, with a smaller time step, boundary merging did not occur and vortex structures remain distinct. To check this result, we halved the sheet length and repeated this calculation. As expected, the findings were identical and the calculations were satisfactory for all three values of C, see Fig. 20. To summarize, in this unsteady regime, more vortices provide better resolution of the large vortex structures; however, there is an accompanying requirement that the

time step be suitably decreased so that the advection error remains small in comparison with the physical diffusion scale. Qualitatively, for a second-order time scheme, the time error is of order Δt^2, and the average jump is proportional to $(\Delta t/R)^{1/2}$, thus we have a rough guide that $R(\Delta t)^{1.5} \leqslant \text{const}$. Since numerous vortex elements are created at the same point on the wall, it is difficult to analyze the relation between the average spacing between elements and C; this is currently under investigation.

Given this analysis of the effect of changing numerical parameters on large-scale eddy structures, we now consider the velocity field itself. Here, we want to study the convergence of the time-averaged velocity profile to see if the same conclusions hold

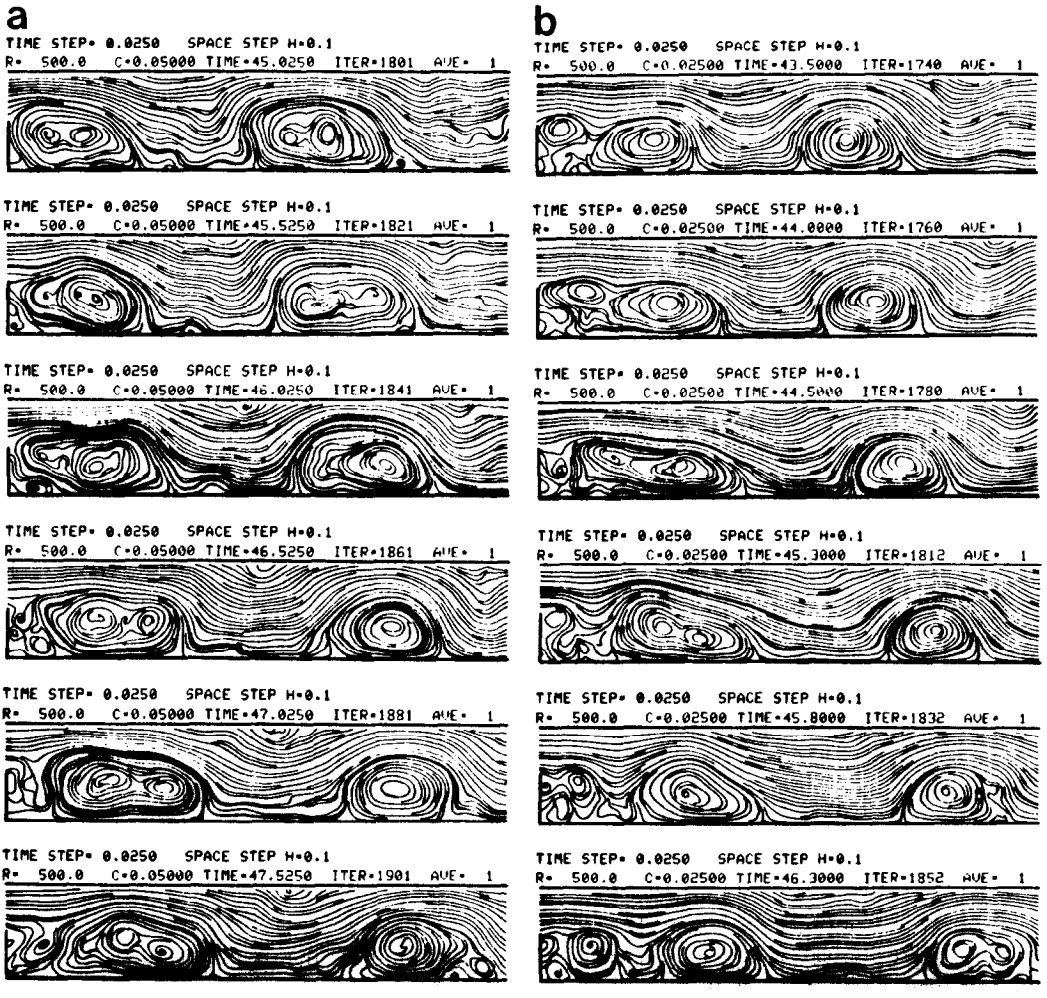

which ends when the center of the third eddy reaches W_{END} and compute the average velocity profile over this second cycle. Do this until all the eddies have been shed in the data set under study, and compute a velocity profile by averaging over all the individual one cycle averages. There were typically 3–4 one cycle averages in each grand average portrait.

In Fig. 21, we show the streamline plots of these average velocity fields for all combinations of $C = 0.05$, 0.025, 0.01, $h = 0.2$, 0.1, and $\Delta t = 0.05$, 0.025. The previous conclusions about the choice of numerical parameters are verified. For the crudest calculations, a jagged, multiple center, single recirculation zone is seen with reattachment length of about 8 step heights. As the number of vortices is increased (C decreased), the average profile becomes a single, smoother, large recirculation zone with a well-defined single center and similar reattachment length. For $C = 0.01$ with $\Delta t = 0.05$ and both $h = 0.2$ and $h = 0.1$, this portrait is lost and the results are ambiguous; but halving the time step ($C = 0.01$, $\Delta t = 0.025$, $h = 0.2$ and $h = 0.1$)

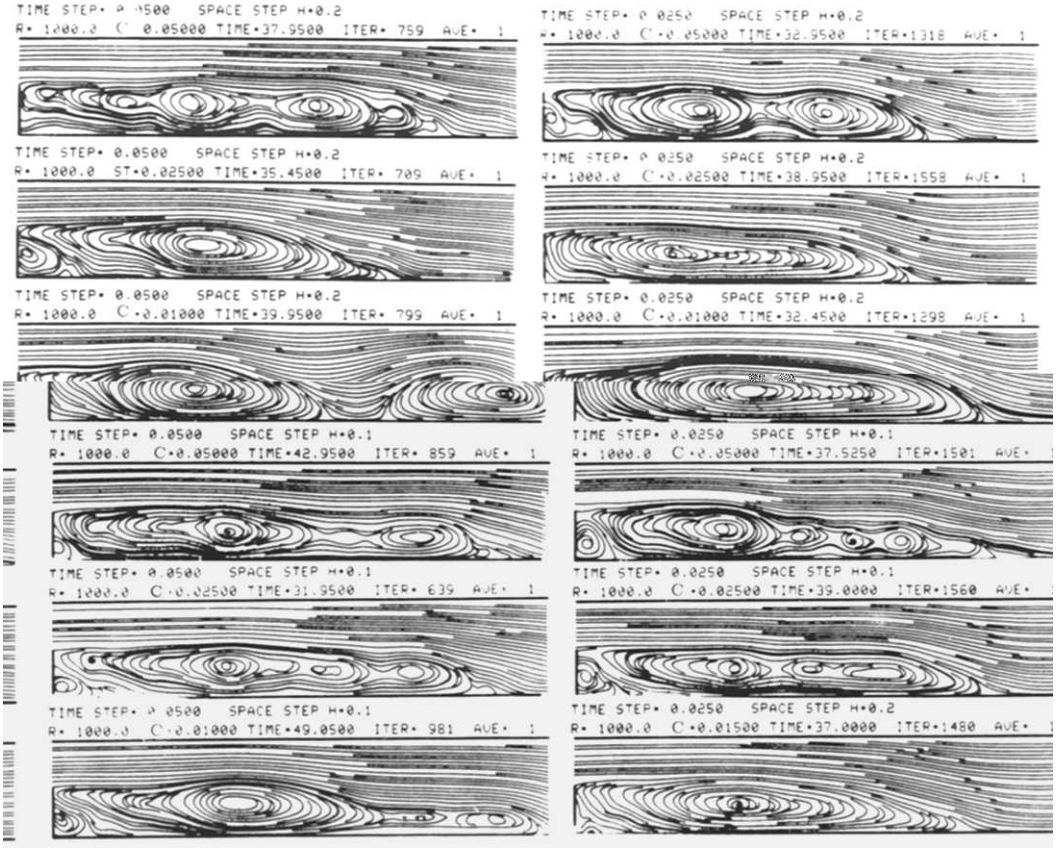

FIG. 21. Average streamlines over one shedding cycle.

brings back the single eddy, single center, smooth recirculation zone with a reattachment length of about 8.5 step heights.

We have been unable to demonstrate the advantage to increasing the number of vortex elements beyong a certain point in higher Reynolds number calculations. Our results show that the global aspects of the solution remains unchanged if the parameter is refined carefully, but presumably, more information is obtained from the additional accuracy. While the real flow is random on the smallest scale, there probably is some regular structure to the medium scales (mid-sized eddies, etc.), however, we have not been able to isolate and identify mechanisms on this scale. Ultimately, we suspect that we need more computational elements to obtain such results.

VII. Summary

We have studied the convergence of the vortex method applied to two-dimensional, viscous, incompressible flow over a backwards-facing step. Calculations were performed over a wide range of Reynolds numbers. At low Reynolds number, where the real solution is steady, we showed that the most important parameter is the circulation of an individual vortex element, which controls the total number N of vortex elements. Within the laminar regime, reductions in the time step and sheet length are of secondary importance. Convergence was demonstrated using a variety of measurements, from integrated quantities such as total circulation to pointwise measurements such as eddy centers and reattachment points. We showed that the variance from the mean decays as $1/N$ for both the velocity field and the total circulation. On the basis of normalized reattachment lengths, we showed excellent agreement with experiment in the calculation of eddy centers, and also showed the essentially linear increase in reattachment length with increasing Reynolds number until the transition regime is reached, at which point the reattachment length is seen to shorten.

For higher Reynolds number calculations, we demonstrated invariance for averaged quantities such as average velocity profiles and eddy boundaries under refinement of numerical parameters. Here, while the total number of vortex elements controlled the accuracy, the time step also must be decreased. With suitable refinement of the relevant numerical parameters, we showed that the dynamics of large fluid structures may be accurately computed. We did not try to analyze our data at high Reynolds number with pointwise instantaneous measurements, since the underlying equations are unstable to small perturbations. The calculations in this paper demonstrate that these perturbations organize themselves into coherent structures whose size and dynamics remain unchanged as the numerical parameters are refined. The problems of identifying, classical and tracking these coherent structures will be discussed in a later paper [40].

ACKNOWLEDGMENTS

The comments and suggestions of Alexandre Chorin, Ole Hald, and the reviewers are gratefully acknowledged. All calculations were performed at the Lawrence Berkeley Laboratory, University of California, Berkeley.

REFERENCES

1. D. E. ABBOT AND S. J. KLINE, *J. Basic Eng.* 317 (1962).
2. C. ANDERSON AND C. GREENGARD, *SIAM J. Numer. Anal.* **22**, 413 (1985).
3. B. F. ARMALY, F. DURST, J. C. F. PEREIRA, AND B. SCHONUNG, *J. Fluid Mech.* **127**, 473 (1983).
4. W. T. ASHURST, in *2nd Symposium on Turbulent Shear Flows*, London, July 1979.
5. J. T. BEALE AND A. MAJDA, *Math. Comput.* **39**, 1 (1982).
6. J. T. BEALE AND A. MAJDA, *Math. Comput.* **39**, 29 (1982).
7. P. BRADSHAW AND F. Y. F. WONG, *J. Fluid Mech.* **52**, 113 (1972).
8. I. P. CASTRO, in *Proceedings, Int. Conf. Num. Meth. in Laminar and Turbulent Flow*, edited by C. Taylor and K. Morgan (Pentech, London, 1978), p. 329.
9. A. Y. CHEER, *SIAM J. Sci. Statist. Comput.* **4**, 685 (1983).
10. A. J. CHORIN, *J. Fluid Mech.* **57**, 785 (1973).
11. A. J. CHORIN, *J. Comput. Phys.* **27**, 428 (1978).
12. V. M. DEL PRETE AND O. H. HALD, *Math. Comput.* **32**, 791 (1978).
13. M. K. DENHAM AND M. A. PATRICK, *Trans. Inst. Chem. Eng.* **52**, 361 (1974).
14. F. DURST AND C. TROPEA, in *Structure of Complex Turbulent Shear Flows, IUTAM Symposium*, edited by R. Dumas and L. Fulachier (Springer-Verlag, Berlin, 1982).
15. J. K. EATON AND J. P. JOHNSTON, in *Turbulent Shear Flows* 3, edited by L. J. S. Bradbury *et al.* (Springer-Verlag, New York 1982).
16. D. W. ETHERIDGE AND P. H. KEMP, *J. Fluid Mech.* **86**, 3, 545 (1978).
17. A. F. GHONIEM, A. J. CHORIN, AND A. K. OPPENHEIM, *Philos. Trans. Soc. London A* **304**, 303 (1982).
18. A. F. GHONIEM AND J. A. SETHIAN, *AIAA J.* **25**, No. 1, 168 (1985).
19. R. J. GOLDSTEIN, V. L. ERIKSEN, R. M. OLSON, E. R. G. ECKERT, *Trans. ASME* 732, (1970).
20. J. GOODMAN, "Convergence of the random vortex method," preprint.
21. L. P. HACKMAN, G. D. RAITHBY, A. B. STRONG, *Int. J. Numer. Method Fluids* **4**, 711 (1984).
22. O. H. HALD, *SIAM J. Numer. Anal.* **16**, 726 (1979).
23. O. H. HALD, *J. Comput. Phys.* **40**, 305 (1981).
24. O. H. HALD, "The flowmap for Euler's equations," preprint.
25. H. HONJI, *J. Fluid Mech.* **69**, 229 (1975).
26. J. P. JOHNSTON, in *Turbulence*, edited by P. Bradshaw (Springer-Verlag, New York/Berlin, 1978).
27. R. KRASNY, *J. Comput. Phys.* **65**, 292 (1986).
28. J. L. KUENY AND G. BINDER, preprint.
29. L. D. LANDAU AND E. M. LIFSHITZ, *Fluid Mechanics* (Pergammon, New York, 1975).
30. A. LEONARD, *J. Comput. Phys.* **37**, 289 (1980).
31. A. LEONARD, in *Annual Review of Fluid Mechanics*, edited by Van Dyke, Wehausen, and Lumley, (Annual Reviews, Palo Alto, CA, 1985).
32. M. A. LESCHZINER, *Computer Methods Appl. Mech. Eng.* **23**, 293 (1980).
33. A. MAJDA AND J. A. SETHIAN, *Combust. Sci. Technol.* **42**, 185 (1985).
34. C. MARCHIORO AND M. PULVIRENTI, *Commun. Math. Phys.* **84**, 483 (1982).
35. M. F. MCCRACKEN AND C. S. PESKIN, *J. Comput. Phys.* **35**, 183 (1980).
36. W. D. MOSS, S. BAKER, L. J. S. BRADBURY, in *Turbulent Shear Flows I*, edited by F. Durst *et al.* (Springer-Verlag, New York/Berlin, 1979).
37. J. PERIAUX, O. PIRONNEAU, AND F. THOMASSET, in *Fifth International GAMM Conference on Numerical Methods in Fluid Mechanics* 1976, (Springer-Verlag, New York/Berlin, 1983).

38. M. PERLMAN, *J. Comput. Phys.* **59**, 200 (1985).
39. S. ROBERTS, *J. Comput. Phys.* **58**, 29 (1985).
40. J. A. SETHIAN, Identifying and tracking coherent structures in turbulent flow, in progress.
41. J. A. SETHIAN, in *Proceedings, Fifth Int. GAMM Conf. Numer. Meth. Fluid Mech., Rome, Italy* (Springer-Verlag, New York/Berlin, 1983).
42. J. A. SETHIAN, *J. Comput. Phys.* **55**, 425 (1984).
43. J. A. SETHIAN AND A. F. GHONIEM, CPAM Report 325, June 1986 (unpublished).
44. J. A. SETHIAN, in *Lectures in Applied Mathematics* Vol. 22 (Amer. Math. Soc., Providence, RI, 1985).
45. J. A. SETHIAN, in *Fire Dynamics and Heat Transfer. Proceedings* 21*st Nat. Heat Transfer Conf.*, edited by J. Quintiere (ASME, New York 1983), p. 29.